Chapter 15
Galactic Demographics: Setting the Scene

I. Neill Reid

15.1 Introduction

Star clusters and associations are the agents for change in galactic environments. They mark locations where the density of the interstellar medium (ISM) was sufficiently high that self-gravity overcame pressure, inducing collapse at multiple locations. Once formed, nuclear processes within the stars generate energy and transform the interior chemical composition. Mass-loss, through winds and more violent phenomena, returns processed material to the ISM, enriching the heavy metal content, generating shocks within neighbouring interstellar clouds that stimulate further star formation and, in some cases, leading to breakout galactic fountains that send material far into the halo and intergalactic medium.

The present series of chapters has three main strands: an examination of the detailed processes involved in how gas within an interstellar cloud redistributes itself to form stars and star systems; an exposition of the dynamical evolution of clusters and associations, paying particular attention to the role of binary and multiple systems; and, finally, a discussion of the general properties of the field population within the Galactic disc, and how those properties can provide insight into the past history of cluster formation within the Milky Way and other galactic systems. To shift metaphors, these three topics form a Russian doll, moving from the spatially compact, short timescale star formation process through medium-scale cluster evolution and dissipation to integration within the large-scale field population, constituting the mix-mastered residue from the long past history of formation and dispersal of star clusters and associations.

My chapters tackle the larger scales. This introductory chapter aims to provide a broad context for the discussion by laying out the basic properties of the Milky Way galaxy and of its component stellar populations. These are wide-ranging topics that

I.N. Reid (✉)
Space Telescope Science Institute, Baltimore, MD, USA
e-mail: inr@stsci.edu

are covered by a broad swathe of the astronomical literature. Rather than trying to provide blanket coverage, my intentions throughout the course are to provide sufficient references to give the interested reader a starting point for further exploration. Apologies in advance to those omitted from explicit citation.

15.2 The Nature of the Milky Way

The Milky Way has been known as a luminous, celestial band for more than 3,000 years. Its popular name derives from the Roman Via Lactea, but it was also the River of Heaven (Al Nahr, Tien Ho, Akash Ganga), a celestial pathway (Waetlinga Straet, Wotan's Way, Winter Street) and, to the Greeks, the Galactic circle or Galaxy. Indeed, a handful of Greek philosophers, including Democritus and, perhaps, Aristotle, even ascribed its diffuse light to a vast congregation of extremely distant stars, an hypothesis that was verified only when Galileo turned his spyglass skywards in 1609.

The original explanation for the congregation of stars known as Milky Way is often ascribed to the Durham clergyman, Thomas Wright, and in his 1750 treatise *An Original Theory or New Hypothesis of the Universe* Wright did suggest that the concentration of stars into a luminous band might reflect geometric projection along a thin, extended distribution. However, Wright envisaged that distribution as a ring-like structure, much like the rings of Saturn. The philosopher Immanuel Kant (1755) and the mathematician, physicist Johann Heinrich Lambert (1761) were the first to independently propose that the Sun lay within an extended disc of stars. Their hypothesis was quantified by William Herschel, who effectively invented the discipline of Galactic astronomy with the star-gaging surveys carried out from Bath in the 1770s. Figure 15.1 shows Herschel's 1785 representation of the local stellar distribution. The strong bifurcated feature is due to the Great Rift in Cygnus; the recognition of the presence of interstellar absorption lay more than a century in the future.
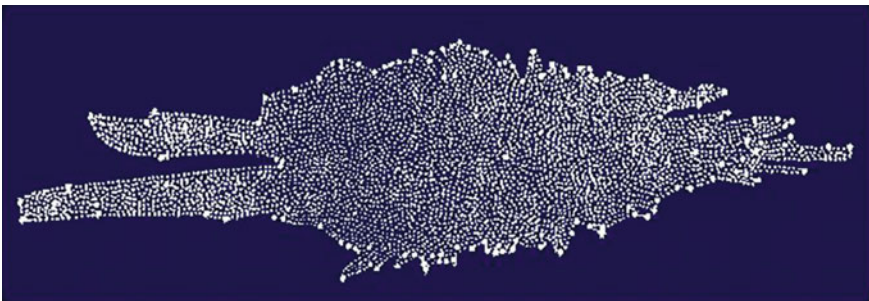
Fig. 15.1 Herschel's model of the Milky Way, deduced from his celestial sweeps and star-gaging. Figure adapted from Herschel (1785)

As part of his celestial sweeps, Herschel encountered numerous diffuse objects and stellar conglomerates. Those nebulae had previously attracted the attention of Edmond Halley, while Charles Messier was in the process of constructing a reference list of the brighter fuzzy objects in support of his main interest of comet hunting. Galileo had argued that closer inspection of such objects would inevitably resolve all as aggregates of faint stars, and such was the case for many systems, notably open clusters like the Pleiades, Praesepe and Messier 67, and globular clusters like Messier 13, 15 and 92. However, even with the development of larger telescopes with greater light grasp and higher resolution, many systems stubbornly resisted resolution.

Herschel constructed his own catalogue of nebulae based on observations with his 20-foot and 40-foot telescopes, eventually compiling a list of 2,500 systems. Herschel's work was taken up and extended to the southern hemisphere by his son, Sir John Herschel, whose General Catalogue included over 5,000 nebulae. By this point, nebulae were classed in three broad categories: gaseous clouds, star clusters and white nebulae. Immanuel Kant had originally suggested that some might prove to be island universes, distant Milky Ways populated by numerous stars. Initially, the elder Herschel subscribed to that viewpoint although his opinions evolved, notably with the discovery of several planetary nebulae. In the latter cases, the diffuse emission was clearly linked to a central star and Herschel came to advocate a close association between nebulae and the star formation process. In contrast, his son fell back on Galileo's suggestion that most, probably all, nebulae would eventually be resolved as star clusters. Herschel's General Catalogue showed a clear deficiency of nebulae within the Milky Way. At the time this was taken as an argument against the island universe hypothesis (where the expectation was a uniform distribution), but this actually reflects dust and absorption in the Galactic Plane.

The General Catalogue was succeeded in 1888 by the New General Catalogue, compiled by John Louis Emil Dreyer, based partly on observations with the 72-inch diameter Leviathan of Parsonstown built by William Parsons, the third Earl of Rosse. During the 1840s, Rosse had used the Leviathan to survey and sketch a number of his nebulae, resulting in the clear detection of spiral structure in several systems, notably Messier 51 (in 1845, the Whirlpool Nebula) and Messier 99 in Coma Berenices (in 1848). The implications were unrecognised, but as photography came to supplant direct visual observations (more of this in Chap. 17), it became evident that many white nebulae shared these morphological characteristics.

The island universe concept received a boost in 1885, with the eruption and subsequent decay of a bright stellar source, S Andromeda, within Messier 31, the Andromeda galaxy. That observation, together with the discovery of novae in other spiral systems, led Heber Curtis of Lick Observatory to espouse that viewpoint. Curtis identified the Milky Way as a relatively small structure, centred near the Sun a concept similar to the model developed by the Dutch astronomer, Jacobus Kapteyn (see Chap. 17). Curtis also noticed that his photographs of spiral systems showed a number with dark bands across the mid-section, which he speculated might be due to dust absorption.

In contrast to Curtis, Harlow Shapley favoured the Big Galaxy hypothesis, envisaging the Sun lying on the outskirts of a single vast system whose centre lay towards

Sagittarius, the centroid of the galactic globular cluster distribution. The two concepts were the subject of the 1919 Great Debate organised by the National Academy of Sciences and designed to address two issues: how large is the Milky Way? and are spiral nebulae island universes? Famously, Shapley and Curtis adopted different speaking styles (populist vs. specialist) and chose to place different emphasis on the two issues, so there was no clear winner at the time. However, Edwin Hubble's subsequent discovery of Cepheid variables in M31 (1923) laid the matter to rest; their distances, estimated using Henrietta Leavitt's period-luminosity relation derived from Magellanic Cloud Cepheids, clearly demonstrated that M31 was not a small stellar aggregate within the confines of even Shapley's Big Galaxy.

Shortly thereafter, the important role played by interstellar absorption within the Milky Way was finally established in a quantitative manner. Dust is largely confined near the Galactic plane. R.J. Trumpler carried out a survey of open star clusters, using the derived Hertzsprung-Russell (H-R) diagrams to estimate distances and hence sizes. Taken at face value, his results suggested that open clusters increased in size with increasing distance, a distinctly non-Copernican result. Trumpler (1930) argued that a more plausible explanation was the existence of material in the line-of-sight that attenuated light from the more distant clusters, giving apparently larger distances. Interstellar absorption was the key ingredient that allowed reconciliation between Shapley's Big Galaxy (which became smaller) and Curtis' island universe.

Island universes come in many forms. As photographic images of galaxies accumulated, morphological patterns started to emerge, leading to the simple tuning-fork classification scheme devised by Edwin Hubble (1926). Galaxies were classed as elliptical (E), spirals (S) and barred spirals (SB). Ellipticals were sub-divided based on their apparent ellipticity (E0 to E7), and spirals as early (Sa/SBa), intermediate (Sb/SBb) or late (Sc/SBc) depending on the relative size of the bulge component (decreasing from Sa to Sc). These regular systems were supplemented by a class of irregular galaxies. Hubble's system has been refined, but still survives as a useful classification and a challenge to galaxy formation models.

Our nearest large neighbor, M31, and its satellite galaxies played a key role in further expanding our understanding of the constituents of the Milky Way, specifically in supporting Walter Baade's development of the stellar population concept. The first clue came from more local observations, as proper motion surveys revealed a handful of stars with extremely high velocities relative to the Sun. Analyses by Lindblad and Oort indicated that the kinematic characteristics were tied to the relative role played by systemic rotation and random motions; high-velocity stars, the subject of Oort's 1926 thesis, were almost exclusively pressure-supported, with negligible rotation.

Further clues came from dwarf galaxies. In 1939, Baade identified Cepheids in the irregular galaxy, IC 1613, placing it at a similar distance to M31, albeit at substantially lower total luminosity. Shortly thereafter, Baade and Hubble identified RR Lyrae variables in the Sculptor and Fornax dwarf galaxies discovered by Shapley. Those systems were similar in size to IC 1613, but the brightest stars were red rather than blue, and they lacked the star-forming regions that were conspicuous in the more distant system. Baade drew explicit comparisons with the Galactic globular clusters.

The clinching data came with Baade's wartime observations of M31 and its companions. Interned as an alien, but retaining his observing privileges on Mt. Wilson as a Carnegie Observatories staff member, Baade took advantage of the blackout conditions to resolve the brightest stars in the central regions of M31 and in its satellites, M32, NGC 195 and NGC 205. Those stars were red, as in the Scuptor and Fornax dwarf galaxies and Galactic globulars, in contrast to the bright blue stars evident in IC 1613 and in M31's spiral arms.

Based on those observations, Baade advanced the concept of distinct stellar populations, namely Population I and Population II. We now know that this distinction represents the dichotomy between an old, evolved stellar population (Population II) and a gas-rich system with on-going star formation, generating short-lived, high-mass stars (Population I). Crucially, Baade demonstrated that this provided a means of characterising the properties of stars within not only the Milky Way, but also other stellar systems. Quoting directly, 'This leads to the further conclusion that the stellar populations of the galaxies fall into two distinct groups, one represented by the well-known HR diagram of the stars in the Solar Neighbourhood (the slow-moving stars), the other by that of the globular clusters. Characteristic of the first group (type I) are highly luminous O- and B-type stars and open clusters; the second (type II), short-period Cepheids (RR Lyraes) and globular clusters. Early-type nebulae (E-Sa) seem to have populations of the pure type II. Both types seem to co-exist in the intermediate and late-type nebulae (Sb-Sc spiral galaxies). The two types of stellar populations had been recognised among the stars of our own Galaxy by Oort as early as 1926.'

Turning to the Milky Way, suggestions that it was itself a spiral galaxy had been made since the late 19th century. Curtis drew an analogy with the spiral nebulae that he photographed from Lick, and that viewpoint gained wider acceptance with identification of Cepheids in the nearby spirals M31 and M33. Baade's results, however, offered a means of settling this question; specifically, the observations that bright OB stars outlined spiral arms suggested that mapping the distribution of such stars in the Milky Way might outline underlying spiral structure. Working with J.J. Nassau, S. Sharpless and D. Osterbrock at Yerkes Observatory, William W. Morgan carried out a photographic survey of most of the northern Milky Way that revealed sections of the features we now know as the Sagittarius arm, the Orion Spur and the Perseus Arm. Presented at the 1951 AAS Christmas meeting, and later supported by HI observations through the nascent radio astronomy program in the Netherlands, the results confirmed the Milky Way as a spiral galaxy and garnered a standing ovation.

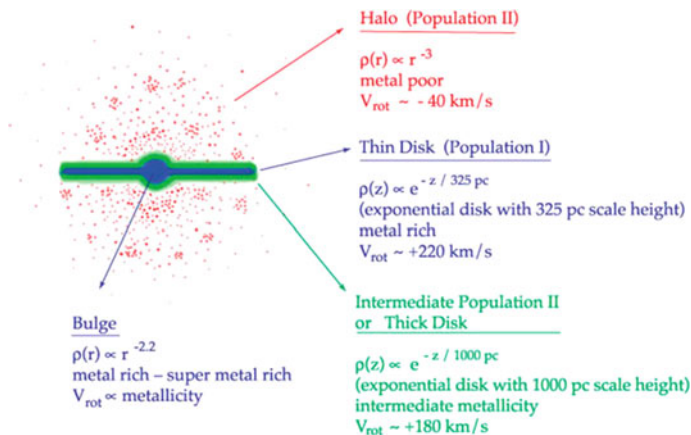## 15.3 The Milky Way as a Galaxy: Large-Scale Properties

What do modern observations reveal about the overall properties of the Milky Way galaxy? Figure 15.2 shows the all-sky map derived from near-infrared (1.25–3.5 μm) observations made by the Diffuse Infrared Background Experiment (DIRBE) on NASA's Cosmic Background Explorer (COBE) mission. Observations at those wave-
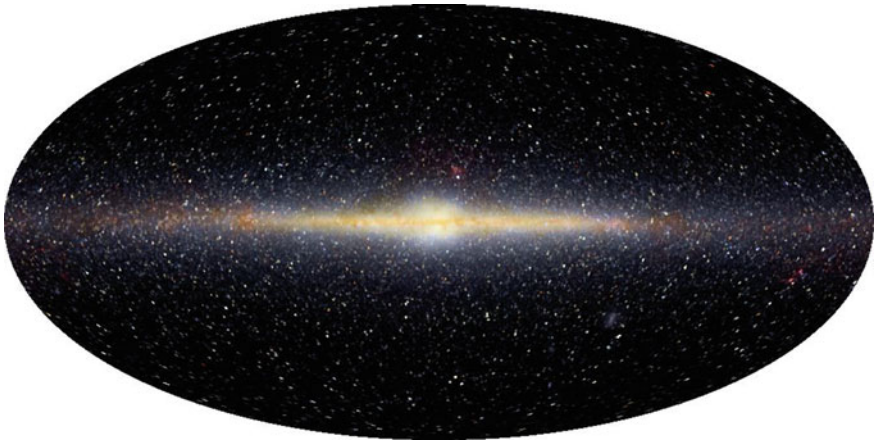
Fig. 15.2 All-sky false-colour near-infrared (1.25, 1.6 and 3.5 μm) map produced by DIRBE/COBE

lengths are dominated by starlight, with some contribution from hot dust. The concentration of stars within the Galactic disc is obvious, as is the boxy/peanut-like central bulge. Detailed star counts towards the bulge strongly suggest the presence of a stellar bar, with consequences for the local kinematics of disc stars (see Chap. 17). The general consensus is that, given an external viewpoint, we would likely classify it as a barred spiral, either type SBc or SBbc. As a comparison, the Andromeda galaxy is also generally classed as Hubble type Sb, while M33 in Triangulum is an Sc galaxy.

The total mass of the Milky Way can be estimated by constructing mass models that take into account constraints imposed by the spatial distribution and kinematics of the Galactic stellar populations and the measured motions of its satellites. The models include the dark matter halo and several baryonic components, including the bulge, the stellar halo and the disc, with the latter usually modelled as two components, thin and thick. Results (Wilkinson and Evans 1999; McMillan 2011) indicate a total mass of $\sim 6 \times 10^{11}\,M_\odot$ within a radius of ~ 60 kpc and a total virial mass ($r < 300$ kpc) of $\sim 1.3 \times 10^{12}\,M_\odot$, with uncertainties of at least a factor 2. Interestingly, applying similar models to M31 indicates that our neighbour is similar in mass, perhaps smaller by $\sim 10\,\%$ (Evans and Wilkinson 2000; Watkins et al. 2010). In any event, baryons are a minority constituent within the Milky Way, $\sim 6.5 \times 10^{10}\,M_\odot$, or less than 5 % of the total mass. The luminosity is estimated as $\sim 2 \times 10^{10}\,L_\odot$ ($M/L \sim 65$) or $M_V \sim -21$ mag; M31's luminosity is estimated as slightly higher, at $\sim 2.6 \times 10^{10}\,L_\odot$ (van den Bergh 1999). This gives the Milky Way a luminosity $L \sim 0.8L_*$, where L_* is the luminosity of a galaxy at the breakpoint in the Schechter (1976) galaxy luminosity function, the transition between a power-law at faint magnitudes and an exponential distribution at bright magnitudes.

Halo (Population II)

$\rho(r) \propto r^{-3}$
metal poor
$V_{rot} \sim -40 \text{ km/s}$

Thin Disk (Population I)

$\rho(z) \propto e^{-z/325\text{ pc}}$
(exponential disk with 325 pc scale height)
metal rich
$V_{rot} \sim +220 \text{ km/s}$

Bulge

$\rho(r) \propto r^{-2.2}$
metal rich – super metal rich
$V_{rot} \propto$ metallicity

Intermediate Population II
or Thick Disk

$\rho(z) \propto e^{-z/1000\text{ pc}}$
(exponential disk with 1000 pc scale height)
intermediate metallicity
$V_{rot} \sim +180 \text{ km/s}$

Fig. 15.3 The Milky Way's stellar population. Figure courtesy of S. Majewski

The spatial distribution and gross characteristics of the constituent stellar populations in the Milky Way are outlined schematically in Fig. 15.3 (see also Freeman and Bland-Hawthorn 2002). The least substantial, and most extended, of these populations is the stellar halo, with a mass of $\sim 4 \times 10^8 \, M_\odot$ (Bell et al. 2008). Its most prominent constituents are globular clusters, of which approximately 130 are currently known. Halo stars form a non-rotating, pressure-supported system with a near-spheroidal distribution, with heavy-element chemical abundances ranging from one-tenth to less than one-ten thousandth that of the Sun. The halo is essentially gas-free, with no evidence for on-going star formation. As discussed further in Chap. 18, these are the local representatives of Baade's Population II, remnants of the Milky Way's first major star formation episode.

Baade originally identified the Galactic Bulge with classical Population II, an identification that appeared to be confirmed with the identification of RR Lyrae variables within his eponymous window. The scarcity of main-sequence stars more massive than the Sun, with only a relatively small number of even A stars identified, indicates a predominantly old population. However, spectroscopic observations have shown that the metal-poor stars within in the Bulge are a minor constituent, probably representing the innermost halo stars. Most Bulge stars are metal-rich, with a significant tail extending to metallicities a factor of 2–3 higher than the Sun (McWilliam and Rich 1994). Its origins remain unclear.

Bulge stars exhibit significant rotation, possibly correlated with metallicity. The visible extent of the Bulge in the DIRBE image corresponds to a diameter of ~ 3 kpc, encompassing the stellar bar (see Chap. 17). The stellar mass is estimated as ~ 1–$2 \times 10^{10} \, M_\odot$ (Kent 1992; Dwek et al. 1995—although note that the latter paper assumes a Salpeter IMF and therefore probably overestimates the contribution of low-mass stars, see Chap. 16). There is evidence for on-going star formation (e.g. the Arches cluster near the Galactic Centre), but this may reflect gas being funnelled from the disc into the central regions and the black hole at the Galactic Centre.

The substantial majority of baryonic material in the Milky Way is in the disc, a flattened, extended, rotationally-supported component with a total mass estimated as 4–5×10^{10} M$_\odot$ (McMillan 2011). Almost all the gas and dust in the Milky Way (and in other spiral galaxies) lies close to the Galactic mid-Plane. Consequently, the disc is the primary location for on-going star formation, most star clusters lie close to the disc, and disc stars are the product of an extensive star-forming history.

Galaxy discs are generally characterised by the presence of extensive, detailed structure, particularly at blue and ultraviolet (UV) wavelengths where young star-forming regions stand out disproportionately. The underlying mass distribution is more regular. Ken Freeman's (1970) seminal analysis of surface photometry of several nearby spiral galaxies showed that the azimuthally-averaged surface brightness profile is well-characterised by an exponential distribution:

$$I(r) = I_\circ r^{ar}, \tag{15.1}$$

where $I_\circ$ is the (extrapolated) central surface brightness and a (also written as hR) is the scalelength, with values of the latter parameters ranging from $\sim$2.5 to 5.5 kpc.

Subsequent analyses, notably by van der Kruit and Searle (1981, 1982), confirmed these results and also indicated that many galaxies showed clear evidence that the radial profile is truncated at 3–5 scalelengths (see Fig. 15.4). This has been inferred as suggesting a cut-off in the star formation process, possibly tied to the gas surface density declining below a critical threshold (van der Kruit and Freeman 2011). However, recent observations, notably with the GALEX satellite, have shown clear evidence for UV light beyond the cut-off radius in some galaxies (e.g. M83, Thilker et al. 2005), in some cases resolved as UV-bright knots. This suggests the presence of on-going star formation, but at a much lower level than within the main body of the disc.
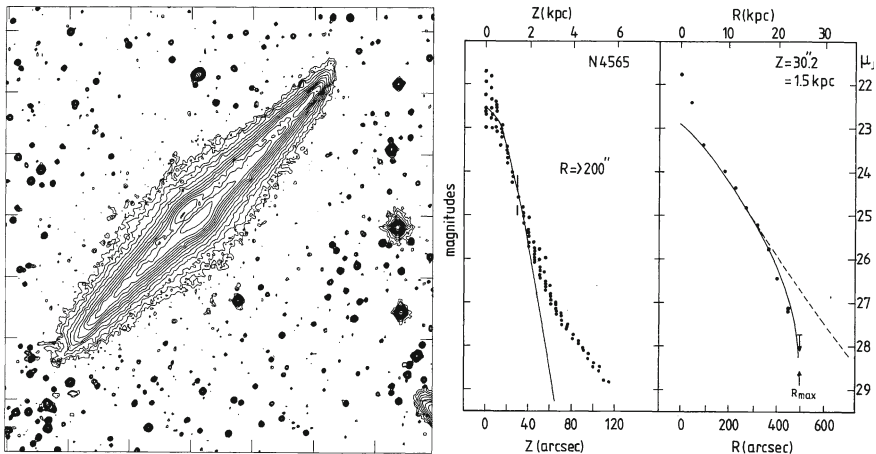
Fig. 15.4 *Left panel*: Surface photometry of the edge-on Sb spiral, NGC 4565. *Right panel*: Derived density profiles along and perpendicular to the disc. Figure adapted from van der Kruit and Searle (1981)

Perpendicular to the disc, many spiral galaxies show evidence for complex density distributions. Close to the mid-Plane, the distribution is well-matched by a simple exponential, but deviations suggestive of the presence of a second component appear at moderate to large heights. This behaviour was noted originally by Burstein (1979), who found that modelling the surface brightness profiles of five S0 galaxies required three components: bulge, disc, and what Burstein termed the 'thick disc'. van der Kruit and Searle (1981, 1982) confirmed that this additional component was required to match some galaxies in their sample (e.g. NGC 4565; see Fig. 15.4), with the additional component generally more prominent in systems with larger bulges.

In the case of the Milky Way, determining the radial density distribution is complicated by our location close to the mid-Plane and the consequent necessity of allowing for interstellar absorption along the line-of-sight both towards and away from the Galactic Centre. Nonetheless, recent analyses suggest that the data are consistent with an exponential scalelength of 2.5–3 kpc (see Table 15.1) and a sharp decline/cut-off in the density distribution ∼6 kpc beyond the Solar radius, or ∼14 kpc from the Galactic Centre (Robin et al. 1992).

Determining the vertical density distribution of the Galactic disc is a more tractable problem. Starcounts show clear evidence for more stars at distances $z > 1.5$ kpc above the Plane than can be modelled with the single exponential associated with disc stars in the 1960s and 70s. As Fig. 15.5 shows, the distribution can be represented using two exponentials characterised as the thin and thick discs, as suggested originally by (Gilmore and Reid 1983). Succeeding years have seen considerable debate regarding both the parameters that should be associated with a two-exponential fit (specifically, the scaleheight and local normalisation of the thick disc) and whether the thin and thick disc are distinct stellar populations, or subsets of an underlying

Table 15.1 Scalelengths and scaleheights for the thin and thick disc

Method	h_R^{thin} (kpc)	h_z^{thin} (pc)	h_R^{thick} (kpc)	h_z^{thick} (pc)	Thick/thin	References
Photographic starcounts		300		1450	2 %	(1)
SEGUE starcounts			4.1 ± 0.4	750 ± 70		(2)
SDSS starcounts	2.6	300	3.6	900	12 %	(3)
2MASS K giant starcounts	3.0 ± 0.1	270 ± 10		1060 ± 50		(4)
Pioneer X flux measurements	4.5–5					(5)
2MASS starcounts	3.7 ± 1.0	360 ± 10	5.0 ± 1.0	1020 ± 30	7 ± 1 %	(6)
Spectroscopic survey			3.4 ± 0.7	695 ± 45		(7)

References: (1) Gilmore and Reid (1983); (2) de Jong et al. (2010); (3) Jurić et al. (2008); (4) Cabrera-Lavers et al. (2005); (5) van der Kruit (1986); (6) Chang et al. (2011); (7) Kordopatis et al. (2011)
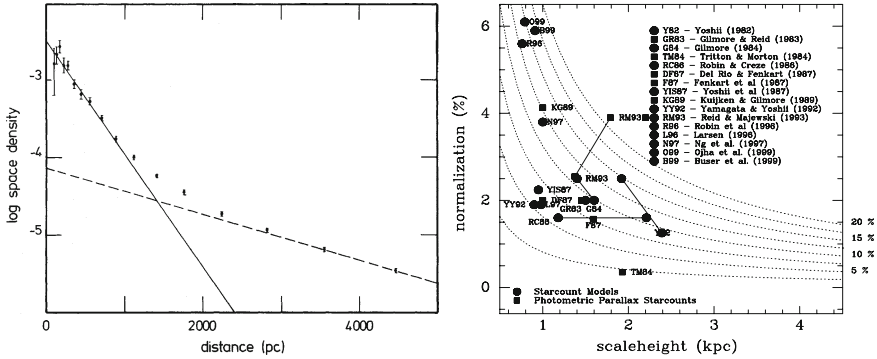
Fig. 15.5 *Left panel*: Two-component fit to star counts towards the South Galactic pole (from Gilmore and Reid 1983). *Right panel*: The various combinations of scale height and local normalisation proposed for the thick disc (from Siegel et al. 2002)

continuum. In other words, is the two-exponential fit simply a mathematical representation, or do these two components have some relation to the underlying physics of galaxy formation? We return to this issue in Chap. 19.

15.4 Star Formation in the Milky Way

Star formation is the key process that drives galaxy evolution. In spiral galaxies like the Milky Way, most star formation is triggered along spiral arms where gas is concentrated by the spiral density wave (illustrated in Fig. 15.6). Gas is shocked and compressed (see Bertin and Lin 1996 for a thorough discussion of this process). The M51 maps show the progression from cold, dense CO clumps, overlying a broader HI distribution, along the inner edge of the arms through the narrow band of Hα associated with HII regions to UV light from OB stars along the outer edge of the arms. The narrow Hα distribution reflects the relative short lifetimes of the high-mass stars that generate ionising radiation. Spiral arms are long-lived, but nonetheless transient features. Density wave patterns are likely to evolve over time and, if so, spiral structure will evolve in a corresponding fashion.

Star formation manifests its presence at many wavelengths across the electromagnetic spectrum (see Fig. 15.7), providing a number of opportunities to measure the global star formation rate within galactic systems. Hot stars register their presence both directly at UV wavelengths (allowing for interstellar absorption) and indirectly, through processed radiation from hot dust, and mid- and far-infrared wavelengths; emission lines due to hydrogen (Hα, Pα) and ionised metals (OII, SII) from ionised gas in HII regions are evident at optical and near-infrared wavelengths; and complex molecular features due to excitation of polycyclic aromatic hydrocarbons (PAHs) are evident at mid-infrared wavelengths. Moving to longer wavelengths, radio emission
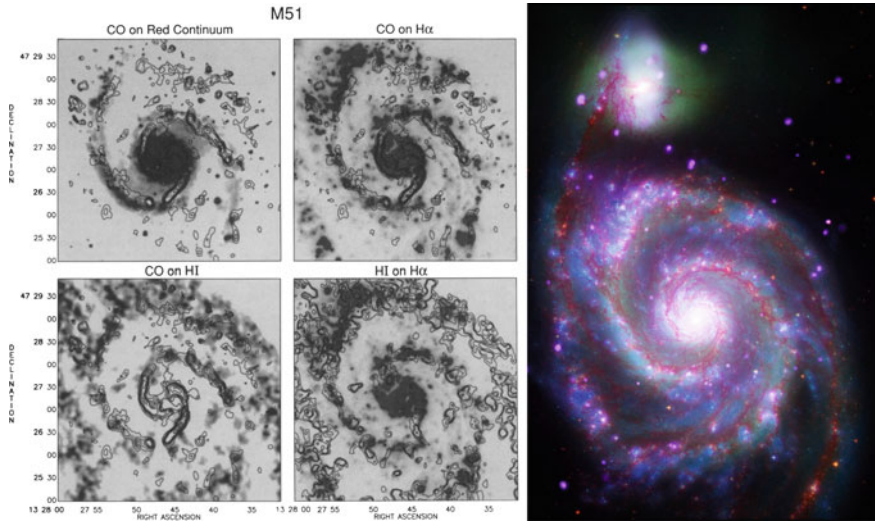
Fig. 15.6 Spiral structure in M51, the Whirlpool galaxy. *Left panel*: Shows cold (CO), warm (HI) and hot (Hα) gas concentrated along the spiral arms (from Rand et al. 1992). *Right panel*: Composite image comprising the following data: *Chandra* X-ray (*purple*), HST optical (*green*), *Spitzer* infrared (*red*) and GALEX UV (*blue*; figure taken from http://thefabweb.com/wp-content/uploads/2012/08/The-Whirlpool-Galaxy-M51-Composite-Image.jpg?25d8db)

Fig. 15.7 Tracing star formation across the electromagnetic spectrum: the spectral energy distribution of the dwarf irregular galaxy, NGC 1705. Figure courtesy of D. Calzetti
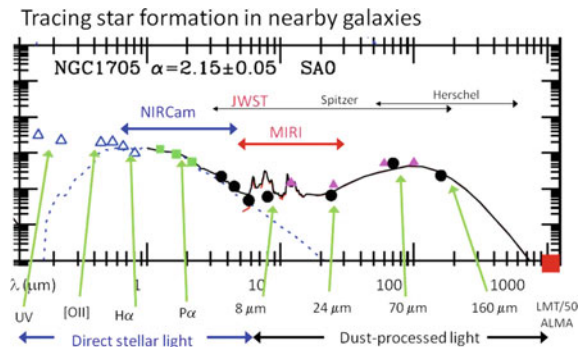
is generated by thermal (free-free emission) and non-thermal processes (synchrotron radiation from cosmic rays generated in supernovae remnants), while, at the other extreme, soft X-rays are generated by thermal emission from gas heated by supernovae and stellar winds from high-mass stars.

Measurements at these wavelengths can be used to estimate the global star formation rates in galactic systems. Calzetti et al. (2009) have reviewed a wide range of methods and summarised the resulting calibrations (their Table 1; reproduced in Fig. 15.8). All of these indicators rely on phenomena associated with *massive* stars, typically exceeding ~ 8–$10\,M_\odot$, while lower-mass stars account for the bulk of mass in star-forming regions. Estimates of the total star formation rate therefore rely on an

Table 1: SFR Calibrations.

| Waveband	SFR ($M_\odot$ yr^{-1})	Comments	Reference
X–ray	$(1.7\pm0.3)\times10^{-40}L_{2-10\ keV}$ (erg s^{-1})	SFR<50 $M_\odot$ yr^{-1}	(1), (2)
	$(8.9\pm1.8)\times10^{-40}L_{2-10\ keV}$ (erg s^{-1})	SFR$\gtrsim$50 $M_\odot$ yr^{-1} or young gals	(2)
	$(1.5\pm0.5)\times10^{-40}L_{0.2-2\ keV}$ (erg s^{-1})		(1)
UV	$(8.1\pm0.9)\times10^{-29}$ l$_\nu$ (erg s^{-1} Hz^{-1})	0.13-0.26 μm range	(3), (4)
Hα	$(5.3\pm1.1)\times10^{-42}$ L(Hα) (erg s^{-1})		(3)
MIR	1.27×10^{-38} [L(24 μm) (erg s^{-1})]$^{0.885}$	L(24 μm)= ν l(ν)	(5), (6)
	5.3×10^{-42} [L(Hα)$_{obs}$ + 0.031 L(24 μm)]	see text	(5), (7)
FIR	3.0×10^{-44} L(8-1000 μm) (erg s^{-1})	see text	(3)
Radio	4.1×10^{-21} $\nu^{0.1}$ l$_{\nu,T}$ (W Hz^{-1})	l$_{\nu,T}$=thermal emiss.	(8)
	3.5×10^{-22} $\nu^{0.8}$ l$_{\nu,NT}$ (W Hz^{-1})	l$_{\nu,NT}$=non–thermal emiss.	(8)
	4.0×10^{-22} l$_{1.4\ GHz}$ (W Hz^{-1})	l$_{1.4\ GHz}$=obs. radio luminosity	(9), (8)

Note. — References: (1) Ranalli et al. 2003; (2) Persic & Rephaeli 2007; (3) Kennicutt 1998; (4) Salim et al. 2007; (5) Calzetti et al. 2007; (6) Alonso–Herrero et al. 2006; (7) Kennicutt et al. 2007; (8) Schmitt et al. 2006; (9) Yun et al. 2001.

Fig. 15.8 Calibrating global star formation rates. Table 1 taken from Calzetti et al. (2009)

assumed form for the underlying initial mass function (IMF, see Chap. 16). In general, higher luminosity galaxies have higher global star formation rates (see Fig. 15.9).

These calibrations can be applied to estimating the global star formation rate in the Milky Way. As with estimates of the radial density distribution, investigations have to make allowance for the presence of dust obscuration in the mid-Plane. Chomiuk and Povich (2011) have reviewed recent analyses based on radio measurements of free-free radiation, far-infrared measurements of dust emission and star counts of OB stars and young stellar objects. Integrating over the disc, they find values ranging from 0.5 to 2.6 $M_\odot$ yr^{-1}, with an average value of 1.9 ± 0.4 $M_\odot$ yr^{-1}. As Fig. 15.9 shows, this value is broadly consistent with the estimated luminosity of the Milk Way.

Star formation is distributed along spiral arms, but the large-scale activity is resolved into a series of smaller scale star-forming events. Table 15.2 lists basic characteristics of different stages in this process. The overall scheme is clear; the details, less so. Star formation becomes apparent within molecular clouds as localised density concentrations that evolve to host (generally) multiple stars. Concentrations of these star-forming clumps are characterised as embedded clusters. As winds from high-mass stars and supernovae clear the remaining gas, the denser embedded clusters emerge as open clusters and the cloud complex as a whole takes on the characteristics of an extended OB association. Clusters dissipate and dissolve with time through gravitational interactions, and globular clusters represent the residuals of the densest star-forming regions from the earliest epochs of galaxy formation. This thumbnail sketch obviously omits a many complications; much more thorough discussions of the physical processes of the star formation and the evolution from embedded clusters to associations and open clusters are given in the chapters presented elsewhere in this volume (see Clarke and Mathieu).
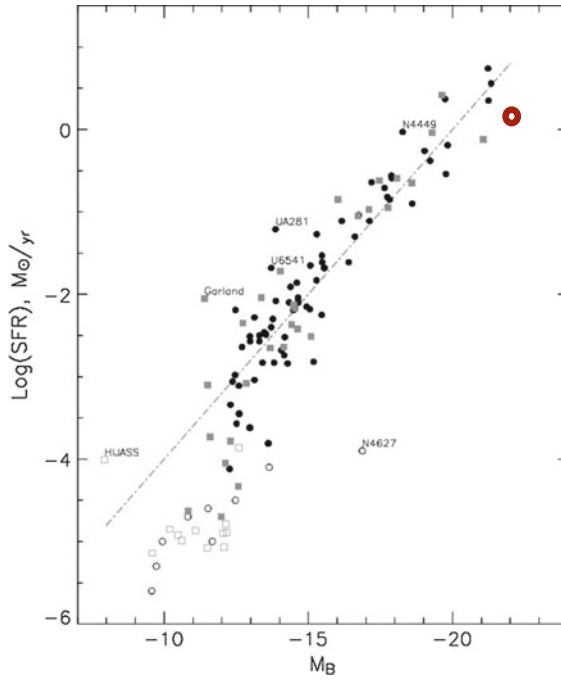
Fig. 15.9 The global star formation rate in spiral galaxies. The Milky Way's location is indicated by the large circle. Figure adapted from Kaisin and Karachentsev (2008)

Table 15.2 Properties of star-forming regions and star clusters

|	Embedded cluster	OB association	Open cluster	Globular cluster
Size	Few–10 pc	20–500 pc	Core radius ∼2 pc	10–40 pc
Mass	100–1000 $M_\odot$	20–80 OB stars	100–1000 $M_\odot$	10^4–10^6 $M_\odot$
Density*	Few stars pc^{-3}	0.1 stars pc^{-3}	∼10–100 stars pc^{-3}	10^3 stars pc^{-3}
Gravitationally bound?	?	No	Yes	Yes
Age	<10 Myr	2–15 Myr	Typically <250 Myr	10–13 Gyr
Numbers		12 within 650 pc	∼3000	∼150

* The star density in these systems can vary substantially; thus, while the average star density in the Orion Nebula Cluster is ∼100 stars pc^{-3}, the core density exceeds 10^4 stars pc^{-3} (Hillenbrand and Hartmann 1998)

15.5 Stellar Abundances

The chemical abundance distribution within galactic systems is driven by the star formation process. Stellar nucleosynthesis transforms hydrogen, helium and light elements to heavy elements, which are returned by mass-loss and winds to the ISM where they contribute to the next generation of star formation. The expectation, therefore, is that the average metallicity of a galaxy increases with time, as more generations of star formation add their nucleosynthetic products to the ISM.

Supernovae are particularly important sources of heavy metals, since that process provides the only means of generating elements heavier than iron. Supernovae come in two main flavours: Type Ia SNe, which are generally believed to be the result of a white dwarf in a binary system accreting sufficient material to exceed the Chandrasekhar mass; and Type II SNe, generated by core collapse in a high mass ($M \gtrsim 7\,M_\odot$) stars. The two processes occur on different timescales and generate ejecta with different abundance distributions: most white dwarf progenitors were intermediate-mass stars, with lifetimes $>1\,$Gyr, and, primarily, they generate elements close to the iron peak; in contrast, massive stars can undergo core collapse within 10–100 Myrs of their formation and have more diverse products, with a high proportion of α-elements (notably O, Ne, Mg, Si, S, Ca), some iron peak, s-process and r-process elements. Since the type II SNe evolve faster, the first few generations of recycled materials include a higher α/Fe abundance ratio than later generations (Matteucci and Greggio 1986), and this becomes evident when one compares the detailed abundance distributions of halo and disc stars (see Fig. 15.10). The overwhelming majority of disc stars, including the Sun, have α-abundances that are a factor of 3–4 lower than in halo stars. Recognising that iron abundance is a chronometer, it becomes clear that the Milky Way enriched its metallicity to close to the solar value within the first 1–2 Gyr of its existence as a star-forming entity.

Fig. 15.10 The evolution of α/Fe abundance ratio as characterised by measurements of calcium abundance in a range of stellar systems. [Fe/H] is the logarithmic abundance of iron relative to hydrogen, scaled to 1 ([Fe/H] $= 0\,$dex) at the solar abundance. Figure adapted from Gratton et al. (2004)
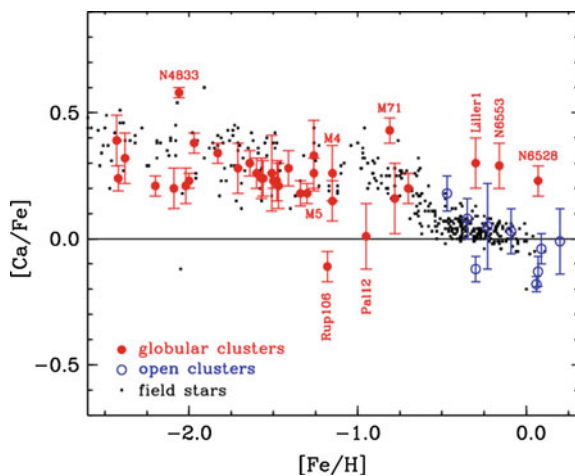
Stellar abundance variations manifest themselves as changes in the relative strength of spectral features. Metallicities are generally measured either through direct analysis of line strengths from spectra, or using narrowband photometric indices designed to sample specific spectral features. In the former case, the spectroscopic line strength measurements are matched against theoretical predictions such as curve of growth analyses or spectral synthesis models. The photometric indices are calibrated empirically, using stars with spectroscopic metallicity determinations. Spectroscopic measurements are more precise than photometric estimates, but are limited to brighter objects by the necessity of acquiring a high signal-to-noise spectrum.

Stellar abundances are measured relative to the Sun and usually given in the form [M/H], where M represents heavy elements (often Fe) and the measurements are in a logarithmic scale. Thus, [Fe/H] $= -1$ dex indicates a stellar abundance of iron that is one-tenth the abundance in the Sun. Extensive observations exist for stars in the vicinity of the Sun, both spectroscopic and photometric (primarily using Strömgren photometry). The results (see Fig. 15.11) reveal an asymmetric distribution that peaks close to the solar value, with an extended tail towards lower abundances. Approximately 40 % of local stars are more metal-rich than the Sun, while less than 5 % have abundances [Fe/H] < -0.5 dex.

Metallicities can also be determined for gaseous nebulae, notably HII regions, using measurements of emission lines produced by neutral and ionised oxygen, carbon and nitrogen. The measurements are in terms of absolute abundances, usually expressed in a logarithmic scale where the abundance of hydrogen is set equal to 12, and provide a particularly effective means of identifying spatial variations in abundance within galaxies. The results indicate that metallicity increases towards

Fig. 15.11 The abundance distribution of field F and G stars in the vicinity of the Sun (from Reid et al. 2007). Note that the distribution peaks close to the Sun's metallicity. Also plotted is the distribution derived by Haywood (2002)
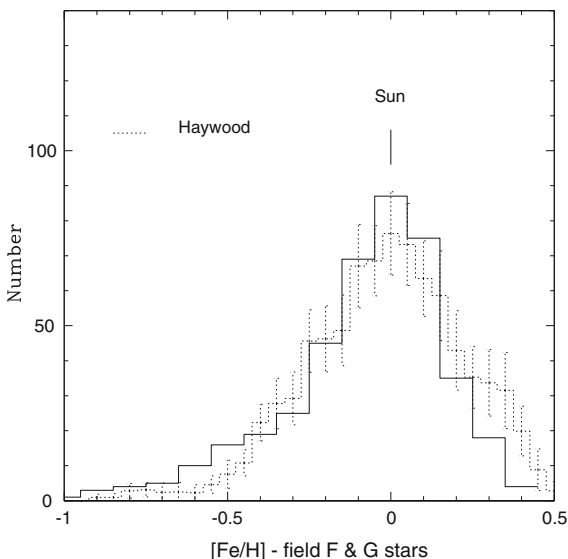
the central regions of the Milky Way and other spirals, with typical gradients of
0.05–0.07 dex kpc^{-1}. Some galaxies (e.g. M33: Cioni 2009) show evidence for a
flattening in the radial variation at large radii. Within the Milky Way, observations of
HII regions or OB stars (both sampling current star-forming regions) are generally
consistent with a slope of ∼0.1 dex kpc^{-1} that may flatten at radii beyond ∼12 kpc
(Smartt et al. 2001; Rudolph et al. 2006). There are sometimes mismatches between
the average abundance of gas and the stars at the same radius, perhaps reflecting
stellar migration (discussed further in Chaps. 17 and 20).

We should highlight an interesting complication regarding the solar metallicity:
oxygen is the third most abundant element in the Sun; despite that fact, consider-
able uncertainty remains over the exact value of the solar oxygen abundance. Until
recently, the standard value was [O] = 8.83 dex, as given by Grevesse and Sauval
(1998). However, detailed line analysis of solar spectra led to proposals reducing that
value by almost two-thirds to 8.66 dex (Asplund 2005). A subsequent re-analysis
leads to a slightly higher value, [O] = 8.69 dex (Asplund et al. 2009). This revision is
not without further implications, since the lower abundance leads to lower opacities
at the base of the convective envelope. That, in turn, leads to sound speeds, density
profiles and helium abundances that are in conflict with helioseismology analyses
(Serenelli et al. 2011). There is, however, possible reconciliation in sight, and we will
return to this issue in Chap. 21. This uncertainty clearly complicates tying the stellar
abundance scale in general, and the Sun's metallicity in particular, to ISM metallic-
ities, which are usually determined by measuring the absolute oxygen abundance in
HII regions.

15.6 The Sun's Place in the Milky Way

The second chapter in this series will concentrate on the properties of the stars, dust
and gas (mainly the stars) within the few tens of parsecs that define the immediate
Solar Neighbourhood. Before focussing in on that scale, it is useful to consider the
Sun's location within the Galaxy from a broader perspective.

The Sun's location vertically within the Galactic Plane is surprisingly well-
determined. Matching starcounts towards the North and South Galactic Poles indi-
cates that the Sun lies somewhat towards the North Pole, offset by 20 ± 0.35 pc
(Humphreys and Larsen 1995). Alternatively, one can map the distribution of young
objects, which are expected to be closely confined in narrow distributions centred on
the mid-Plane. Observations of Cepheids indicate an offset of 26±3 pc (Majaess et al.
2009); OB stars give 19.6 ± 2.1 pc (Reed 2000); and measurements of open clusters
indicate 22.8 ± 3.3 pc (Joshi 2005). Overall, the results are remarkably consistent,
placing the Sun ∼20 pc above the mid-Plane of the Galactic disc.

The Sun's distance from the Galactic Centre, the Solar Radius or R$_o$, has been
determined using a variety of techniques. Observations of distance indicators such
as RR Lyraes and Type II Cepheids allow estimates of the distance to the centroid of
the Bulge, giving values of 8.1 ± 0.6 and 7.7 ± 0.7 kpc, respectively (Majaess 2010;

Majaess et al. 2009). Alternatively, proper motion measurements of objects near or at the Galactic Centre can be used to estimate the distance, since the apparent motion reflects the Sun's orbital velocity around the Galactic Centre. Measurements of OH masers in high-mass star-forming regions give a value of 8.24 ± 0.55 kpc. Direct measurement of the radio source Sgr A* give values of 8.0 ± 0.4 kpc (Ghez et al. 2008) and 8.33 ± 0.35 kpc (Gillessen et al. 2009). Overall, the various indicators indicate that $R_\circ \sim 8.0$ kpc, with an uncertainty of 5%. As noted above, the stellar density distribution in the disc shows a sharp decrease approximately 6 kpc beyond the Sun's orbit, implying a total radial extent of ~14 kpc.

Focusing on the local environment, the Sun lies in an interarm region relatively close to the star-forming feature known as the Orion Spur, which itself lies between the inner Sagittarius spiral arm and the outer Perseus arm (see Fig. 15.12). Zooming in to a scale of a few hundred parsecs (see Fig. 15.13), it becomes apparent that the Sun is in a quiescent region. The nearest active star-forming regions (ρ Ophiuchus, Chamaelon, Taurus and the Scorpius-Centaurus association) and their associated molecular clouds are more than 150 pc from the Sun. The nearest open clusters are the Hyades (age ~ 650 Myr, distance ~ 50 pc), the Pleiades (age ~ 130 Myr, distance ~ 130 pc) and Praesepe (age ~ 650 Myr, distance ~ 180 pc). There are relatively few stars younger than the Pleiades in the immediate vicinity of the Sun. Nonetheless, with that caveat, the stars populating the Solar Neighbourhood represent a fair sampling of the stellar content of the Galactic disc, a subject pursued further in the next chapter.

Fig. 15.12 The Sun's location within the Milky Way. The major spiral arm features and the Galactic Bar are labelled. Figure from Momany et al. (2006)
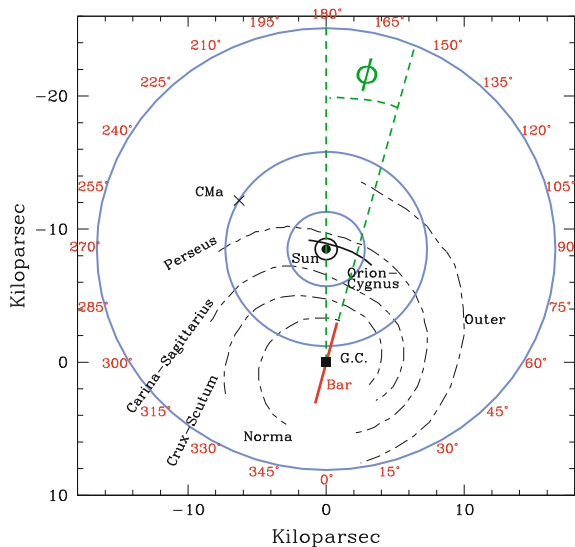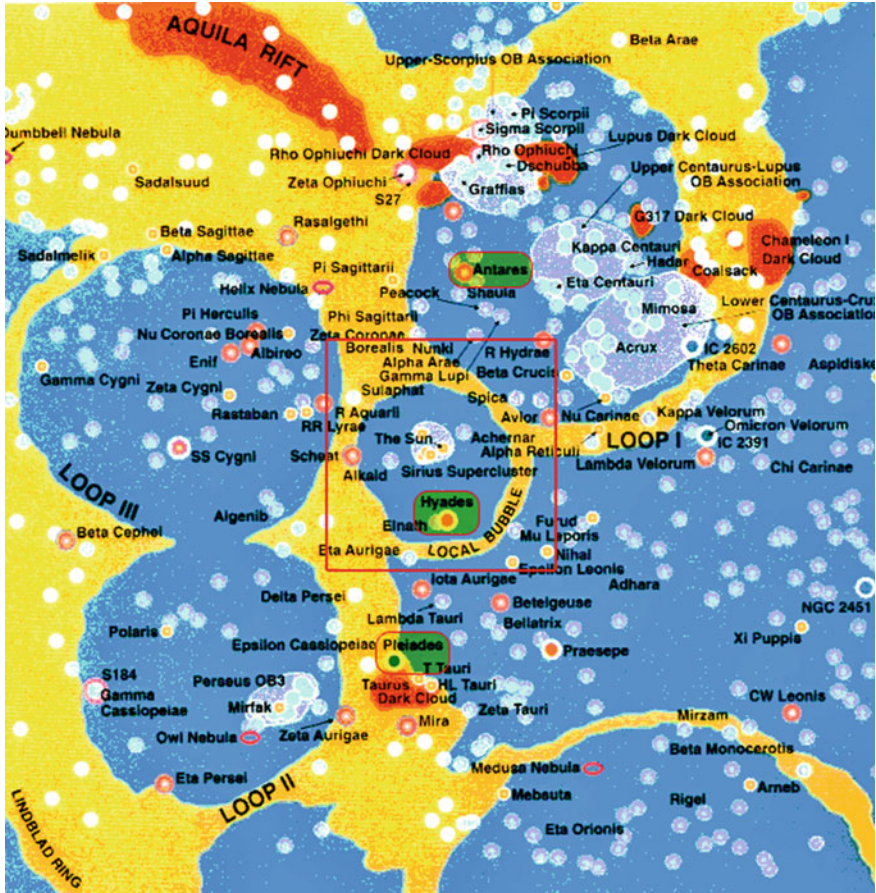
Fig. 15.13 A map of the ∼400 × 400 pc region centred on the Sun. Shaded areas map higher gas density, star-forming regions. The Galactic Centre lies at ∼12 o'clock in this diagram, while the Hyades cluster lies in the direction of the Galactic anticentre. Figure from Henbest and Couper (1994)

References

Asplund, M. 2005, ARA&A, 43, 481

Asplund, M., Grevesse, N., Sauval, A. J., & Scott, P. 2009, ARA&A, 47, 481

Bell, E. F., Zucker, D. B., Belokurov, V., et al. 2008, ApJ, 680, 295

Bertin, G. & Lin, C. C. 1996, Spiral Structure in Galaxies: A Density Wave Theory, ed. Bertin, G. and Lin, C. C., MIT Press.

Burstein, D. 1979, ApJ, 234, 829

Cabrera-Lavers, A., Garzón, F., & Hammersley, P. L. 2005, A&A, 433, 173

Calzetti, D., Sheth, K., Churchwell, E., & Jackson, J. 2009, in The Evolving ISM in the Milky Way and Nearby Galaxies, ed. K. Sheth, A. Noriega-Crespo, J. Ingalls, & R. Paladini.

Chang, C.-K., Ko, C.-M., & Peng, T.-H. 2011, ApJ, 740, 34

Chomiuk, L. & Povich, M. S. 2011, AJ, 142, 197

Cioni, M.-R. L. 2009, A&A, 506, 1137

de Jong, J. T. A., Yanny, B., Rix, H.-W., et al. 2010, ApJ, 714, 663

Dwek, E., Arendt, R. G., Hauser, M. G., et al. 1995, ApJ, 445, 716

Evans, N. W. & Wilkinson, M. I. 2000, MNRAS, 316, 929

Freeman, K. C. 1970, ApJ, 160, 811

Freeman, K. & Bland-Hawthorn, J. 2002, ARA&A, 40, 487

Ghez, A. M., Salim, S., Weinberg, N. N., et al. 2008, ApJ, 689, 1044

Gillessen, S., Eisenhauer, F., Trippe, S., et al. 2009, ApJ, 692, 1075

Gilmore, G. & Reid, N. 1983, MNRAS, 202, 1025

Gratton, R., Sneden, C., & Carretta, E. 2004, ARA&A, 42, 385

Grevesse, N. & Sauval, A. J. 1998, Space Sci. Rev., 85, 161

Haywood, M. 2002, MNRAS, 337, 151

Henbest, N. & Couper, H. 1994, The Guide to the Galaxy, ed. Henbest, N. and Couper, H., Cambridge
    University Press.

Herschel, W. 1785, Royal Society of London Philosophical Transactions Series I, 75, 213.

Hillenbrand, L. A. & Hartmann, L. W. 1998, ApJ, 492, 540

Hubble, E. P. 1926, ApJ, 64, 321

Humphreys, R. M. & Larsen, J. A. 1995, AJ, 110, 2183

Joshi, Y. C. 2005, MNRAS, 362, 1259

Jurić, M., Ivezić, Ž., Brooks, A., et al. 2008, ApJ, 673, 864

Kant, I., 1755, Allgemeine Naturgeschichte und Theorie des Himmels (Königsberg and Leipzig,
    Germany)

Kaisin, S. S. & Karachentsev, I. D. 2008, A&A, 479, 603

Kent, S. M. 1992, ApJ, 387, 181

Kordopatis, G., Recio-Blanco, A., de Laverny, P., et al. 2011, A&A, 535, 107

Lambert, J. H., 1761, Cosmologische Briefe uber die Einrichtung des Waltbaues (Augsburg, Ger-
    many)

Majaess, D. 2010, AcA, 60, 55

Majaess, D. J., Turner, D. G., & Lane, D. J. 2009, MNRAS, 398, 263

Matteucci, F. & Greggio, L. 1986, A&A, 154, 279

McMillan, P. J. 2011, MNRAS, 414, 2446

McWilliam, A. & Rich, R. M. 1994, ApJS, 91, 749

Momany, Y., Zaggia, S., Gilmore, G., et al. 2006, A&A, 451, 515

Rand, R. J., Kulkarni, S. R., & Rice, W. 1992, ApJ, 390, 66

Reed, B. C. 2000, AJ, 120, 314

Reid, I. N., Turner, E. L., Turnbull, M. C., Mountain, M., & Valenti, J. A. 2007, ApJ, 665, 767

Robin, A. C., Creze, M., & Mohan, V. 1992, ApJ, 400, L25

Rudolph, A. L., Fich, M., Bell, G. R., et al. 2006, ApJS, 162, 346

Schechter, P. 1976, ApJ, 203, 297

Serenelli, A. M., Haxton, W. C., & Peña-Garay, C. 2011, ApJ, 743, 24

Siegel, M. H., Majewski, S. R., Reid, I. N., & Thompson, I. B. 2002, ApJ, 578, 151

Smartt, S. J., Venn, K. A., Dufton, P. L., et al. 2001, A&A, 367, 86

Thilker, D. A., Bianchi, L., Boissier, S., et al. 2005, ApJ, 619, L79

Trumpler, R. J. 1930, PASP, 42, 214

van den Bergh, S. 1999, JRASC, 93, 200

van der Kruit, P. C. 1986, A&A, 157, 230

van der Kruit, P. C. & Freeman, K. C. 2011, ARA&A, 49, 301

van der Kruit, P. C. & Searle, L. 1981, A&A, 95, 105

van der Kruit, P. C. & Searle, L. 1982, A&A, 110, 61

Watkins, L. L., Evans, N. W., & An, J. H. 2010, MNRAS, 406, 264

Wilkinson, M. I. & Evans, N. W. 1999, MNRAS, 310, 645